# Rise time of proton cut-off energy in 2D and 3D PIC simulations

J. Babaei,[1] L. A. Gizzi,[2] P. Londrillo,[3] S. Mirzanejad,[1] T. Rovelli,[4] S. Sinigardi,[4,a)] and G. Turchetti[5]

[1]*Department of Physics, Faculty of Basic Sciences, University of Mazandaran, P.O. Box 47415-416, Babolsar, Iran*
[2]*ILIL, Istituto Nazionale di Ottica, CNR Pisa and INFN Sezione di Pisa, Italy*
[3]*INAF Osservatorio Astronomico di Bologna, Via Ranzani 1, 40127 Bologna, Italy*
[4]*Dipartimento di Fisica e Astronomia, Università di Bologna and INFN Sezione di Bologna, Via Irnerio 46, I-40126 Bologna (BO), Italy*
[5]*Dipartimento di Fisica e Astronomia, Università di Bologna, Via Irnerio 46, I-40126 Bologna (BO), Italy*

The Target Normal Sheath Acceleration regime for proton acceleration by laser pulses is experimentally consolidated and fairly well understood. However, uncertainties remain in the analysis of particle-in-cell simulation results. The energy spectrum is exponential with a cut-off, but the maximum energy depends on the simulation time, following different laws in two and three dimensional (2D, 3D) PIC simulations so that the determination of an asymptotic value has some arbitrariness. We propose two empirical laws for the rise time of the cut-off energy in 2D and 3D PIC simulations, suggested by a model in which the proton acceleration is due to a surface charge distribution on the target rear side. The kinetic energy of the protons that we obtain follows two distinct laws, which appear to be nicely satisfied by PIC simulations, for a model target given by a uniform foil plus a contaminant layer that is hydrogen-rich. The laws depend on two parameters: the scaling time, at which the energy starts to rise, and the asymptotic cut-off energy. The values of the cut-off energy, obtained by fitting 2D and 3D simulations for the same target and laser pulse configuration, are comparable. This suggests that parametric scans can be performed with 2D simulations since 3D ones are computationally very expensive, delegating their role only to a correspondence check. In this paper, the simulations are carried out with the PIC code ALaDyn by changing the target thickness $L$ and the incidence angle $\alpha$, with a fixed $a_0 = 3$. A monotonic dependence, on $L$ for normal incidence and on $\alpha$ for fixed $L$, is found, as in the experimental results for high temporal contrast pulses. *Published by AIP Publishing.* [http://dx.doi.org/10.1063/1.4979901]

## I. INTRODUCTION

The acceleration of protons by intense laser pulses is still the subject of active experimental investigation. The most consolidated regime is the Target Normal Sheath Acceleration (TNSA), where the electrons, heated by a laser, diffuse and leave the target, creating an electric field which accelerates the surface protons present in the contaminants. The comparison with current particle-in-cell (PIC) simulations is still affected by uncertainties. Indeed, the energy spectra are found to be exponential with a cut-off

$$\begin{cases} dN/dE = (E_{\max}/T)\ e^{-E/T} & \text{for } E < E_{\max} \\ dN/dE = 0 & \text{for } E > E_{\max}, \end{cases}$$

but the cut-off energy $E_{\max}$ and the average energy $T$ (proton temperature) depend on time. In 2D PIC TNSA simulations, a monotonic rise of $E_{\max}$ with time is observed, whereas in 3D PIC, a slow trend towards a possible saturation to an asymptotic value is usually observed. As a consequence, a comparison of 2D (two dimensional) and 3D (three dimensional) simulations is difficult since the laws of the cut-off energy rise with time $E_{\max}(t)$ appear to be different.

Although the different asymptotic dependence on $t$ for $E_{\max}$ for 2D and 3D PIC simulations is well known, its origin

has not been investigated. Empirical rules, based on a choice of $t$ related to laser pulse duration $\tau_L$, have been proposed, and the ratio between the 3D and 2D cut-off energies has been suggested to be $\sim 2/3$. To our knowledge, no model was proposed to explain this behaviour. A logarithmic growth of the proton energy was shown to occur in a plasma vacuum expansion model, but no relation with PIC simulations was suggested. A comparison of 2D and 3D simulations was presented in the literature for a model of composite targets (foam+metal target),[1] but the problem of the different asymptotic behaviour of $E_{\max}$ was not addressed. Another systematic study, using 2D and 3D simulation, was presented for thin solid targets down to the transparency limit and for near critical targets.[2] In both cases, the acceleration regime is not TNSA, the way the cut-off energies in 2D and 3D are determined is not specified, and a model to relate them is not proposed.

In this paper, we try to give a phenomenological answer to this question, by proposing two empirical laws for $E_{\max}(t)$, which are suggested by a model first proposed by Schreiber *et al.*,[3] to describe the dependence of the cut-off energy from the laser pulse duration.

Schreiber's model refers to a 3D configuration, and we worked out its 2D version obtaining an analytic approximation to the cut-off energy dependence on time. Both in 2D and 3D, the cut-off energy $E_{\max}(t)$ depends only on two parameters, the rise time $t^*$, and the asymptotic energy $E_\infty$.

a)sinigardi@bo.infn.it

This model assumes that the hot electron cloud leaves the rear side of the target, creating a surface density of positive charge, whose electric field accelerates the protons belonging to the contaminants. For a Gaussian laser pulse of waist $R$, we have considered a 2D model in which the surface charge is located on a strip, with the infinite length and height $2R$, and a 3D model in which the surface charge is located on a disc of radius $R$. In our model, the laser is assumed to have normal incidence on the target and in Figure 1, we sketch the geometric configurations.

The numerical analysis presented here refers to a laser pulse with $\tau = 40\,\text{fs}$ and $a_0 = 3$. This choice was made because, recently, systematic experiments with such a laser pulse were carried out at ILIL in Pisa.[4] Furthermore, several experiments with similar parameters, which ensure that the acceleration regime is TNSA, are present in the literature. For an overview on the physics of the proton acceleration by high intensity lasers and related experiments, we refer to recent reviews.[5–7] In the intensity range that we have considered, experimental results concerning the dependence on the target thickness, the incidence angle, and the temporal contrast are reported in many papers.[8–14] When the contrast is very high, the cut-off energy varies monotonically with target thickness and if the contrast were infinite, this behaviour should be observed, until the radiation pressure becomes dominant by approaching the relativistic transparency limit. When the contrast is finite, as in experiments, a maximum in the cut-off energy $E_{max}$ is reached by decreasing the metal foil thickness. Further reducing it, a rapid decrease to zero of $E_{max}$ is observed due to the increasing damage on the foil

induced by the prepulse. A significant dependence on the incidence angle is also observed, and typically, the proton cut-off energy increases with the angle up to a maximum value because the electrons are heated more efficiently.[6]

In our model, the preplasma is neglected (the temporal contrast is assumed as infinite). Because of this choice, the Amplified Spontaneous Emission (ASE) prepulse is not permitted. On the other hand, a prepulse coming from compression artefacts (ps time scale) can be tolerated when comparing our simulation results with experiments, as long as the plasma preformed on the illuminated side of the target has a scale length much shorter than the laser wavelength.

The 2D and 3D simulations were carried out with the ALaDyn code,[15] and the asymptotic cut-off energy $E_\infty$ was determined by a best-fit procedure on its time dependence, following the laws obtained from the electrostatic model, which just depend on two parameters: the asymptotic cut-off energy $E_\infty$ and the rise time $t^*$, i.e., the time at which the energy starts to rise.

Beyond the good agreement of the asymptotic cut-off energies obtained from 2D and 3D simulations, the monotonic dependence on the incidence angle and the target thickness was found to be in qualitative agreement with the experimental results for high contrast pulses.

In our 3D simulations, the transverse section of the computational box is the same as the target, whose extension is comparable with the focal spot (four times bigger) measured by the waist. As a consequence, a leakage of electrons from the computational box occurs and when the fraction of lost electrons becomes appreciable, typically for $ct$ significantly above $100\,\mu\text{m}$, the simulation loses reliability. That is why we stop our analysis at this time. Increasing the box size would enable us to go further but without adding any insightful detail.

Our method allows us to limit the simulation even to $ct = 60\sim80\,\mu\text{m}$ using small boxes since the results are already stable and comparable with 3D results. Here, we present the results for a single laser pulse and various target thicknesses, to assess the validity of our model, even though we have started a more extensive exploration by varying the laser duration, its intensity, and the metal target electron density. A detailed analysis of the dependence of $E_\infty$ and $t^*$ on laser and target parameters will give us a better insight, but, from the encouraging results obtained so far, we can conclude that the simple method we propose here appears to be adequate to extract the asymptotic cut-off energy from PIC simulations.

## II. THE 3D CASE

Starting from the 3D case and considering a laser pulse which propagates along the $z$ axis, we choose an electrostatic potential which vanishes at $z = 0$, where a uniform charge density $\sigma$, within a disc of radius $R$, is located. This potential is given by
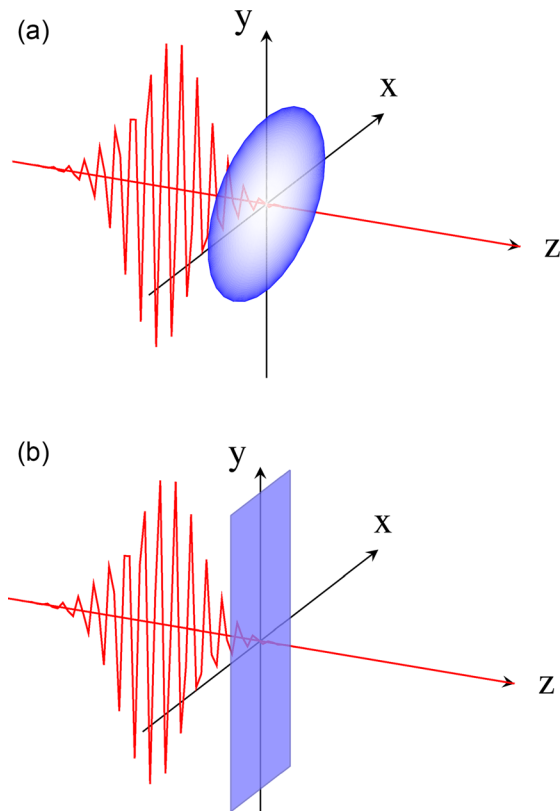


FIG. 1. Schematic representation of the configurations used to compute the accelerating field: 3D (top) and 2D (bottom).

$$V(\zeta) = 2\pi R\,\sigma\left(\sqrt{1 + \zeta^2} - \zeta - 1\right) \quad \zeta = \frac{z}{R}.$$

Asymptotically, for $z \to \infty$, it behaves as $V = Q/z$, where $Q = \pi R^2 \sigma$ is the charge on the disc. A particle initially at rest accelerates, and the law of motion is obtained from energy conservation. Since $V(0) = 0$, we have

$$m\frac{v^2}{2} + eV(z) = 0 \quad v = \dot{z}.$$

Letting $v_\infty = \dot{z}(\infty)$, the kinetic energy of the particle, after integrating the equation of motion, is

$$E(t) \simeq E_\infty \left(1 - \frac{t^*}{t}\right)^2 \quad t > t^* = \frac{R}{4v_\infty},$$

where

$$E_\infty = m\frac{v_\infty^2}{2} = 2\pi e R \sigma.$$

Since this is an asymptotic law, we may assume that $E(t) = 0$ for $t < t^*$. Notice that $E$ is the highest energy reached at time $t$, namely, $E = E_{max}$.

## III. THE 2D CASE

In this case, we have an infinite strip along the $y$ axis with uniform charge density $\sigma$ on $-R < x < R$. A potential that vanishes at $z = 0$ is given by

$$V(z) = 4R\sigma\left(-\zeta \arctan\frac{1}{\zeta} + \log\frac{1}{\sqrt{1 + \zeta^2}}\right)$$
$$\simeq -4R\sigma \log(1 + \zeta),$$

where we defined $\zeta = z/R$. To obtain this result, it is simpler to compute first the electric field $\mathcal{E}_x = 4\sigma \arctan(1/\zeta)$, whose asymptotic behaviour is $4\sigma/\zeta$. As a consequence, a potential having this asymptotic behaviour and which vanishes at the origin is $\hat{V} \simeq -4R\sigma \log(1 + \zeta)$. The potential in this case diverges logarithmically, and consequently, the particle accelerates indefinitely. We approximate the potential energy with

$$e\hat{V}(z) = -E_\infty \log(1 + \zeta), \quad E_\infty \equiv m\frac{v_\infty^2}{2} = 4eR\sigma.$$

We may then easily solve the equations of motion from energy conservation, assuming the proton are initially at rest in the origin as for the 3D case. The result is (see the [Appendix](#) for more details)

$$E(t) = E_\infty \log\left(\frac{t}{t^*}\right) \quad t \geq t^* = \frac{R}{v_\infty}.$$

Again, since this is an asymptotic law, we may assume that $E(t) = 0$ for $t < t^*$.

## IV. COMPARISON WITH PIC SIMULATIONS

Even though the models we propose are very simple, we tried to see whether the predicted asymptotic laws for $E(t)$ hold for PIC simulations. The answer is positive, at least for targets consisting of a uniform foil whose thickness is in the micrometer range, covered by a thin layer of contaminants. For this type of targets, the fits, both for 2D and 3D PIC simulations, are surprisingly accurate. However, the asymptotic energy $E_\infty$ and the time scale $t^*$ in 2D and 3D must be considered fitting parameters, even though the results we obtain have the correct order of magnitude with respect to the theoretical results.

The law to be fitted for 2D simulations is

$$\begin{cases} E_{max}^{(2D)}(ct) = 0 & \text{for } t < t^{*(2D)} \\ E_{max}^{(2D)}(ct) = E_\infty^{(2D)} \log\frac{ct}{ct^*} & \text{for } t > t^{*(2D)}. \end{cases}$$

We perform a linear fit by defining $y = E$ and $x = \log ct$ so that the previous law becomes

$$y = a + bx, \quad E_\infty^{(2D)} = b, \quad ct^{*(2D)} = e^{-a/b}.$$

The law to be fitted for 3D simulations is

$$\begin{cases} E_{max}^{(3D)}(ct) = 0 & \text{for } t < t^{*(3D)} \\ E_{max}^{(3D)}(ct) = E_\infty^{(3D)}\left(1 - \frac{ct^{*(3D)}}{ct}\right)^2 & \text{for } t > t^{*(3D)}. \end{cases}$$

We can perform a linear fit by defining $y = \sqrt{E}$ and $x = 1/ct$ so that the previous law becomes

$$y = a + bx, \quad E_\infty^{(3D)} = a^2, \quad ct^{*(3D)} = -\frac{b}{a}.$$

## V. RESULTS FOR 2D SIMULATIONS

We have considered the following model: the laser pulse has wavelength $\lambda = 0.8\,\mu m$, intensity $I = 2 \times 10^{19}\,W/cm^2$, waist $6.2\,\mu m$, and P-polarization and its duration is $40\,fs$. The corresponding normalized vector potential is $a_0 = 3$. The target is a uniform Al foil of thickness $L$ varying between 0.5 and $8\,\mu m$, having a layer of hydrogen on the rear (nonilluminated) side, with a fixed thickness of $0.08\,\mu m$.

The ionization levels are $Al^{9+}$ and $H^+$, and it is fixed throughout the simulation. The electron densities have been chosen as $n_e^{Al} = 100\,n_c$ and $n_e^H = 10\,n_c$. For an Al foil, whose thickness is in the range of 0.5–8 $\mu m$, we expect that the process is dominated by TNSA (we are far above the transparency limit). The collisions have been neglected in our simulations.

In Figure 2, we show the results obtained from 2D simulations for $0.5\mu m \leq L \leq 8\mu m$, by plotting $E_{max}(ct)$ in a linear and a logarithmic scale for $ct$ with the corresponding fits. In Table I, we quote the results of the fit: we notice that $E_\infty^{(2D)} \simeq E(ct = 50)$. In Figure 3, we resume the dependence of the cut-off energy on the thickness. In Figure 4, we show the results of 2D simulations obtained when the incidence angle is small but different from zero: the logarithmic growth in $ct$ is still present, and the linear fits are quite good; see also Table II, where the numeric values for $\alpha = 5°$, $10°$, and $15°$, and a target thickness of $L = 2\,\mu m$ are shown.
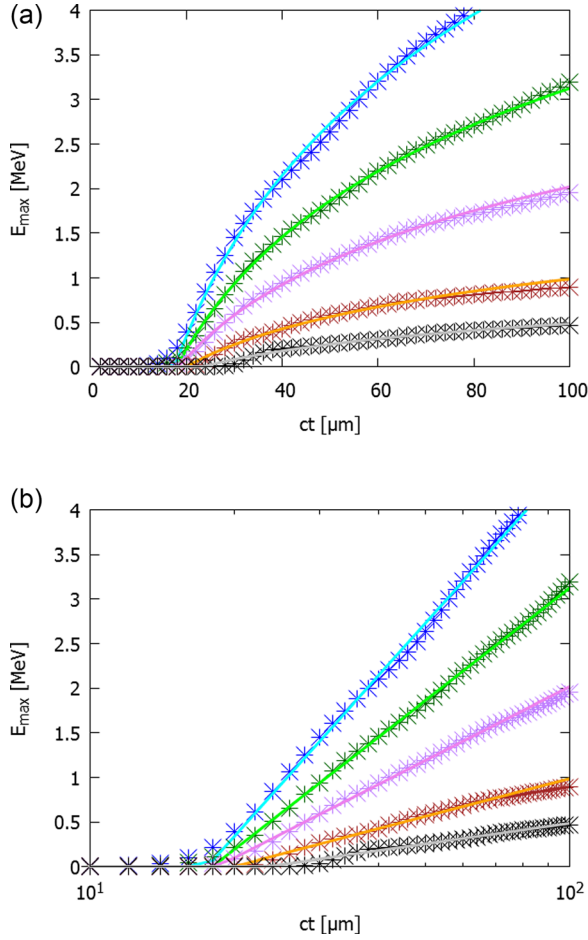
(a)



(b)

FIG. 2. (Top) Cut-off energy $E_{\max}$ versus $ct$ in the range $10 \leq ct \leq 100 \ \mu$m obtained from a PIC simulation (stars) and comparison with the fit (continuous line) for targets of various thicknesses $L$. Blue (cyan), $L = 0.5 \ \mu$m; dark green (green), $L = 1 \ \mu$m; purple (violet), $L = 2 \ \mu$m; brown (orange), $L = 4 \ \mu$m; and black (grey), $L = 8 \ \mu$m. (Bottom) The same as the upper panel but on a logarithmic scale for $ct$, which clearly shows the linearity and the accuracy of the fit.

TABLE I. Fitting parameters for 2D simulations with zero incidence angle and target thicknesses $0.5 \leq L \leq 8 \ \mu$m. The chosen intervals for fitting are $ct_1 = 20 \ \mu$m and $ct_2 = 80 \ \mu$m.

| $L$ | $E_{\max} (ct = 50)$ | $E_\infty^{(2D)}$ | $ct*^{(2D)}$ | $\sigma_E$ | $\sigma_{ct*}$ |
|-----|-----|-----|-----|-----|-----|
| 0.5 | 2.64 | 2.62 | 17.5 | 0.05 | 0.03 |
| 1 | 1.82 | 1.82 | 18.0 | 0.02 | 0.15 |
| 2 | 1.19 | 1.19 | 18.4 | 0.02 | 0.2 |
| 4 | 0.58 | 0.61 | 19.9 | 0.02 | 0.5 |
| 8 | 0.25 | 0.33 | 23.3 | 0.02 | 0.9 |

## VI. RESULTS FOR 3D SIMULATIONS

We present now the results for some 3D simulations, precisely with $L = 0.5$, 1, and 2 $\mu$m. In Figure 5, we show the curves corresponding to a linear fit to $\sqrt{E(t)}$ versus $1/ct$. The asymptotic values $E_\infty^{(3D)}$ and the fitting curves up to $ct = 100 \ \mu$m are shown in the upper panel of Figure 5.

We notice that, even though the extrapolated data from the 2D and 3D simulations are not the same, the correspondence is quite reasonable. In Table III, the numerical results are quoted, and in any case, the discrepancy does not exceed
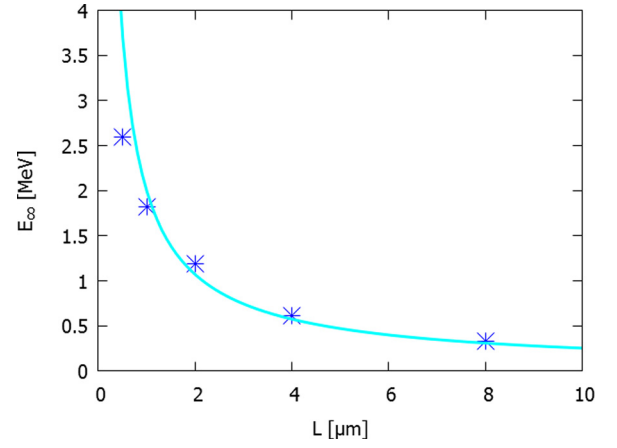


FIG. 3. Comparison of the extrapolated cut-off energy for 2D PIC simulations (blue stars) for different target thicknesses $L = 0.5$, 1, 2, 4, and 8 $\mu$m and a fit with the curve $E_{\max} = 1/L^{0.9}$ (cyan line).

20%. We may observe that the energy for $ct = 50 \ \mu$m in the 2D simulation is very close to the extrapolated value, due to the logarithmic growth, but in 3D, at $ct = 50 \ \mu$m, the energy value is less than one half of the extrapolated value $E_\infty$, due to the slower rise. In this case, there is an asymptotic limit,
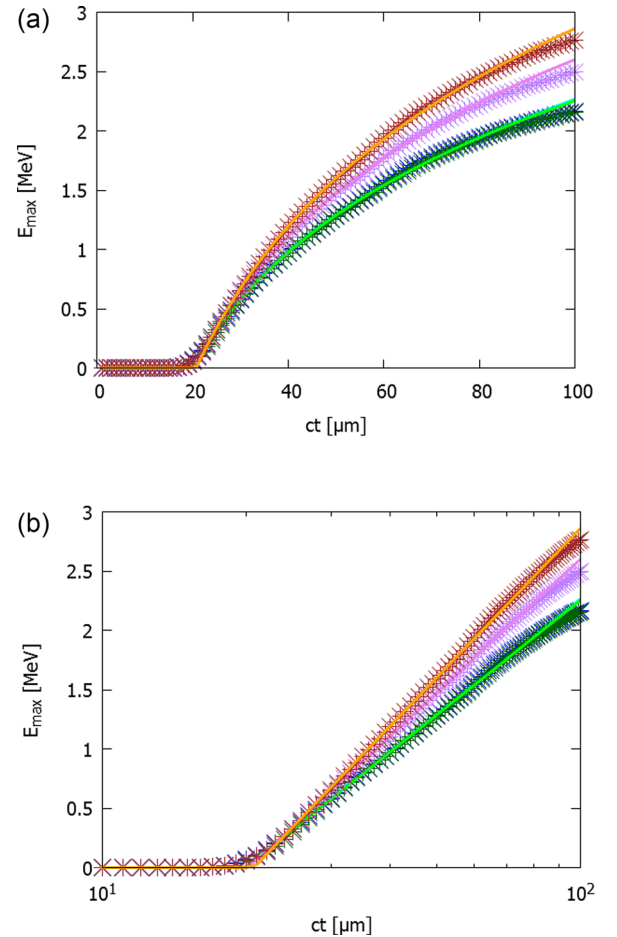


(a)



(b)

FIG. 4. (Top) Comparison of the 2D PIC solution with a small incidence angle $\alpha$. The figure shows $E_{\max}$ versus $ct$, with the stars corresponding to the PIC simulation and the curves to the fit for various angles: $\alpha = 5°$, dark green (green); $\alpha = 10°$, purple (violet); and $\alpha = 15°$, brown (orange). (Bottom) The same data are plotted with a logarithmic scale for $ct$, which shows how the data stay on a line and the accuracy of the linear fit (Table II).

TABLE II. Fitting parameters for 2D simulations for three different incidence angles $\alpha = 5°$, $10°$, and $15°$ and target thickness $L = 2\,\mu m$. The chosen intervals for fitting are $ct_1 = 20\,\mu m$ and $ct_2 = 80\,\mu m$, and the fitting errors are quoted.

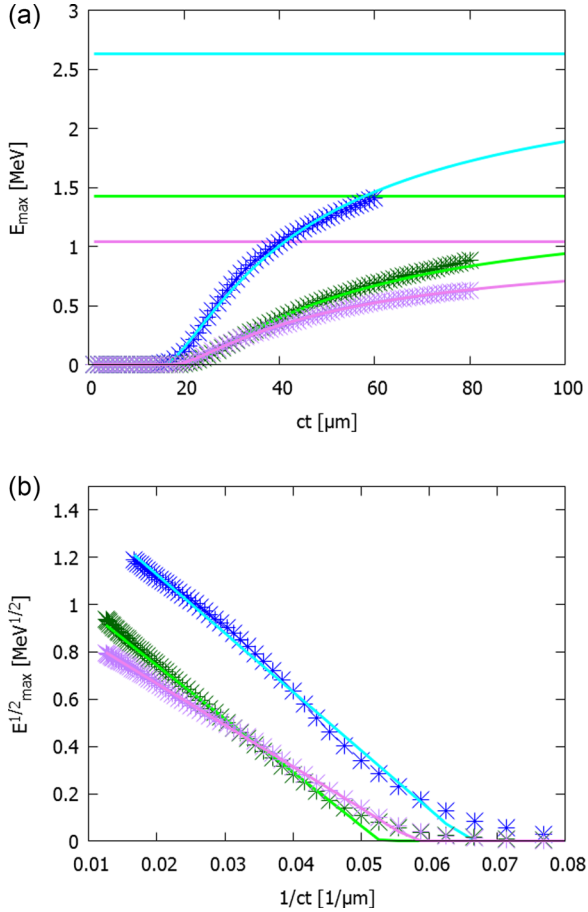| $\alpha$ | $E_{max}$ ($ct = 50$) | $E_\infty^{(2D)}$ | $ct^{*(2D)}$ | $\sigma_E$ | $\sigma_{ct^*}$ |
|---|---|---|---|---|---|
| 5 | 1.28 | 1.40 | 19.9 | 0.01 | 0.1 |
| 10 | 1.47 | 1.62 | 20.1 | 0.01 | 0.1 |
| 15 | 1.59 | 1.82 | 20.7 | 0.02 | 0.15 |



FIG. 5. (Top) Results for a 3D PIC simulation for $E_{max}$ versus $ct$ (stars) compared with the linear fit of $\sqrt{E_{max}}$ as a function of $1/ct$ (continuous lines, and the asymptotic values $E_\infty^{(3D)}$ are also shown), for different target thicknesses: $L = 0.5\,\mu m$, blue (cyan); $L = 1\,\mu m$, dark green (green); and $L = 2\,\mu m$, purple (violet). (Bottom) Plot of $\sqrt{E_{max}}$ versus $1/ct$, which shows their linearity, with the corresponding linear fit.

TABLE III. Fitting parameters for 3D simulations for zero incidence angle and three different target thicknesses $L = 0.5$, 1, and $2\,\mu m$. The chosen intervals for fitting are $ct_1 = 20\,\mu m$ and $ct_2 = 60\,\mu m$, and the fitting errors are quoted.

| $L$ | $E_{max}$ ($ct = 50$) | $E_\infty^{(3D)}$ | $ct^{*(3D)}$ | $\sigma_E$ | $\sigma_{ct^*}$ |
|---|---|---|---|---|---|
| 0.5 | 1.25 | 2.63 | 15.3 | 0.01 | 0.2 |
| 1 | 0.56 | 1.43 | 18.9 | 0.02 | 0.1 |
| 2 | 0.44 | 1.04 | 17.3 | 0.01 | 0.1 |

which is reached quite far, when $ct > 200\,\mu m$. Such a large value is computationally too expensive to be attained, but a correct extrapolation is still possible with data just up to $ct \lesssim 50\,\mu m$.

The comparison with the experimental results is a challenging task: in Figure 6, we show the results of some experiments whose laser pulse has the same P-polarization, with a duration and intensity very close to the ones considered here and whose target has the same structure, namely, a metal foil plus contaminants. The cut-off energy increases as the target thickness is reduced, until the effect of finite contrast prevails inverting the trend. The results of various experiments differ by more than a factor two, but the decreasing trend is similar, and the same behaviour can be seen in the 2D and 3D PIC simulations.

## VII. CONCLUSIONS

The asymptotic value of the cut-off energy of protons, which is what is measured in experiments, is difficult to extract from PIC simulations. Indeed, the 2D results do not exhibit a saturation, whereas the 3D results show that a saturation might be reached, despite at a large time ($ct > 200\,\mu m$), which is computationally too expensive to be reached. We propose here a simple recipe based on the model described by Schreiber *et al.*,[3] which assumes that the acceleration of protons present in the contaminants is due to the positive surface charge created on the rear target, thanks to the escape of the electrons. In the 3D version, the charged spot is circular with a radius $R$ comparable with laser waist. The rise in time of the cut-off energy can be analytically computed. We have formulated an analogous 2D model where the charge is on an infinite strip of height $2R$, and we obtain a simple asymptotic expression for the rise in time of the cut-off energy, which does not saturate but exhibits a logarithmic growth, just as in 1D models of the vacuum expansion of plasmas.[16] The analytical results suggest two phenomenological laws, which depend on the asymptotic energy $E_\infty$ and the time $t^*$ at which the acceleration begins. The fits to the 2D and 3D results coming from PIC simulations are quite good, and the statistical uncertainties $\sigma_{E_\infty}/E_\infty$ and $\sigma_{ct^*}/ct^*$ are quite small (a few percent).
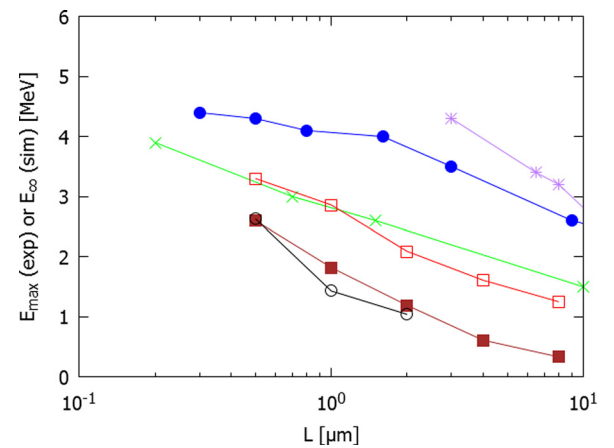


FIG. 6. Plot of $E_{max}$ versus $L$ on a logarithmic scale from various experiments with a laser pulse having $a_0 \sim 3$ and a metal target: the Ceccotti experiment (45° incidence angle) from Ref. 9 (blue circles), Neely experiment (30°) from Ref. 12 (green crosses), and Flacco experiment (45°) from Ref. 14 (purple stars). These data are compared with the results of our 2D PIC simulation at zero degree incidence (filled red squares) and at 30° incidence (empty red squares) and 3D PIC simulation at zero degree incidence (empty black circles).

The extrapolated values $E_\infty^{(2D)}$ and $E_\infty^{(3D)}$, computed for different target thicknesses, are comparable, and moreover, they can be fully calculated fitting the results obtained before $ct \lesssim 50$–$60\,\mu m$, which is a distance reachable also in 3D numerical simulations. There is no need to let simulations run longer since the fit can already be correctly obtained. The fitting appears to be satisfactory also for small incidence angles, even though the model was developed for normal incidence.

To conclude, we believe that, for the targets that we have analysed, in which the protons are only on the thin layer above the bulk, the proposed phenomenological model is adequate to avoid the arbitrariness in the choice of the time at which the asymptotic cut-off energy is chosen in numerical simulations. In addition, the parametric explorations, which can be carried out only in 2D, may have a quantitative value, with an adequate extrapolation, rather than being of purely qualitative nature. The results we have presented refer to a specific intensity and a range of target thicknesses chosen in order to fulfil the applicability conditions of the model.

## ACKNOWLEDGMENTS

## APPENDIX: ASYMPTOTIC CUT-OFF ENERGY ANALYTICAL ESTIMATES

Let us consider a target which is infinitely extended along the plane $xy$ and delimited by the planes $z = -L$ and $z = 0$. We can consider a circular radius $r_L$ which we assume to be the spot of the laser pulse propagating along $z$. The electrons are heated and diffused by the laser itself. Supposing that they diverge with angle $\theta$, the electrons will leave the plane $z = 0$ from a disc of radius

$$R = r_L + L \tan\theta.$$

We assume that the target is a metallic foil and that the protons are in the contaminants deposited on the plane $z = 0$. The electrons, which are heated, diffuse and cross the $z = 0$ boundary, leaving the target and inducing on it a positive charge density $\sigma(t)$, which we suppose varies slowly with $t$. If $Qe$ is the total number of positive charge on the surface, the density is

$$\sigma = \frac{Qe}{\pi R^2}. \tag{A1}$$

This is the geometry for the 3D case, which we shall treat analytically.

We consider another geometry in which the electrons on the plane $z = L$ leave the rectangle $|x| \leq R$, $|y| \leq L$ of area $4LR$. In this case, the density is given by

$$\sigma = \frac{Qe}{4RL}. \tag{A2}$$

The intensity defined as the power per unit surface is assumed to be the same for both geometries.

### A. The 3D case: Charge density on a disk

Using cylindrical coordinates and computing the potential, we have

$$V(z) = 2\pi\sigma \int_0^R r\,dr\,\frac{1}{\sqrt{r^2 + z^2}} = \pi\sigma \int_0^R dr^2\,\frac{1}{\sqrt{z^2 + r^2}}$$
$$= 2\pi\sigma\left[\sqrt{z^2 + R^2} - z\right].$$

Introducing the dimensionless variable $\zeta = z/R$, we have

$$V(\zeta) = 2\pi R\sigma\left[\sqrt{1 + \zeta^2} - \zeta\right].$$

Since $V(0) = 2\pi R\sigma$, we redefine the potential by subtracting it.

$$\hat{V}(\zeta) = V(\zeta) - V(0) = 2\pi R\sigma\left[\sqrt{1 + \zeta^2} - \zeta - 1\right]. \tag{A3}$$

The potential energy is given by $eV(\zeta)$. We notice that we have

$$\begin{cases} \hat{V}(z) \simeq -2\pi\sigma z & \text{for } z \to 0 \\ \hat{V}(z) \simeq \dfrac{eQ}{z} - \dfrac{2Qe}{R} & \text{for } z \to \infty. \end{cases}$$

Letting $v = \dot{z}$ and assuming $v(0) = 0$, i.e., that the protons are initially at rest on the surface $z = 0$, we can apply the energy conservation

$$m\frac{v^2}{2} + eV(\zeta) \equiv E + eV(\zeta) = 0.$$

Calling $v_\infty$, the speed reached at infinite distance

$$E_\infty = m\frac{v_\infty^2}{2} = -eV(\infty) = \frac{2Qe^2}{R} = 2\pi\,e\,R\,\sigma,$$

we can define

$$-eV(\zeta) = 2\pi\,e\,R\sigma\,s(\zeta) = m\frac{v_\infty^2}{2}s(\zeta),$$

where from Equation (A3)

$$s(\zeta) = 1 + \zeta - \sqrt{1 + \zeta^2}.$$

As a consequence, we have

$$E = E_\infty s(\zeta), \quad v = v_\infty\sqrt{s(\zeta)}. \tag{A4}$$

We introduce the new variables

$$X = \sqrt{s}, \quad \tau = t\frac{v_\infty}{R}.$$

Then, we have

$$\frac{d\zeta}{d\tau} = \frac{v}{v_\infty} = \sqrt{s(\zeta)}. \tag{A5}$$

We might solve this equation with initial condition $\zeta(0) = 0$. We rather solve the equation for $X$

$$\frac{dX}{d\tau} = \frac{dX}{ds}\frac{ds}{d\zeta}\frac{d\zeta}{d\tau} = \frac{1}{2}\frac{ds}{d\zeta}. \tag{A6}$$

Let us notice that

$$\frac{dX}{d\tau} = \frac{1}{2}\left(1 - \frac{\zeta}{\sqrt{1 + \zeta^2}}\right) = \frac{1}{2}\left(1 + \frac{\zeta}{1 - s}\right)^{-1}.$$

Inverting $s = s(\zeta)$, we have $\zeta = (2s - s^2)/(2(1 - s))$, and finally replacing this in the r.h.s. of the last equation, we obtain

$$\frac{dX}{d\tau} = \left(1 + \frac{1}{(1 - s)^2}\right)^{-1} = \left(1 + \frac{1}{(1 - X^2)^2}\right)^{-1}.$$

The results are obtained with integration by parts

$$\begin{aligned}
\tau &= X + \int_0^X \frac{du}{(1 - u^2)^2} \\
&= X - \frac{1}{2}\frac{d}{d\alpha}\int_0^X \frac{1}{\alpha^2 - u^2}\bigg|_{\alpha=1} \\
&= X + \frac{1}{2}\frac{X}{1 - X^2} + \frac{1}{4}\log\frac{1 + X}{1 - X}.
\end{aligned}$$

Asymptotically, for $\tau \to \infty$, we have $X \to 1$

$$\tau \sim \frac{1}{4(1 - X)}, \quad X \simeq 1 - \frac{1}{4\tau}.$$

The energy asymptotic behaviour is given by $E/E_\infty = s = X^2$, and consequently for $t \to \infty$

$$E \simeq E_\infty\left(1 - \frac{1}{4\tau}\right)^2.$$

## B. The 2D case: Charge on slab

We consider the slab $|x| \leq R$ and $|y| \leq L$ on the rear surface $z = 0$, where the density is given by Eq. (A2). The potential is given by

$$\begin{aligned}
V(z) &= \sigma\int_{-R}^R dx \int_{-L}^L \frac{dy}{\sqrt{x^2 + y^2 + z^2}} \\
&= 4\sigma\int_0^R dx \int_0^{L/\sqrt{x^2 + z^2}} \frac{du}{\sqrt{1 + u^2}} \\
&= 4\sigma\int_0^R dx\, \text{arsinh}\left(\frac{L}{\sqrt{x^2 + z^2}}\right). \tag{A7}
\end{aligned}$$

Since $4\sigma = eQ/(LR)$, we first consider the limit $L \to 0$, which corresponds to the density $\sigma(z) = eQ/(2R)\delta(y)$, and the result, letting $\zeta = z/R$, is

$$V(z) = \frac{eQ}{R}\int_0^R dx\left(\frac{1}{\sqrt{x^2 + z^2}}\right) = \frac{eQ}{R}\,\text{arsinh}\frac{1}{\zeta}.$$

Recalling that $\text{arsinh}(u) = \log(u + \sqrt{1 + u^2})$, we see that $V(\zeta) \sim \log(2/\zeta)$ for $\zeta \to 0$, whereas it vanishes as $1/\zeta$ for $\zeta \to \infty$. As a consequence, we cannot have $V$ vanishing at $\zeta = 0$ with a subtraction. Indeed, if we compute $V(0)$, we will see that it diverges as $\log(1/L)$ for $L \to 0$ (see Eq. (A10)). We wish to define a potential which vanishes at $z = 0$: as a consequence, in the definition, we have to subtract $V(0)$. This can be done for any finite value of $L$ and also for $L \to \infty$. In order to compute $V(0)$ for a given non vanishing $L$, we set $\xi = x/L$; integrating by parts, we obtain

$$\begin{aligned}
V(0) &= \frac{eQ}{R}\int_0^{R/L} d\xi\,\text{arsinh}\frac{1}{\xi} \\
&= \frac{eQ}{R}\left[\xi\,\text{arsinh}\frac{1}{\xi}\bigg|_0^{R/L} + \int_0^{R/L}\frac{d\xi}{\sqrt{1 + \xi^2}}\right] \\
&= \frac{eQ}{R}\left[\frac{R}{L}\,\text{arsinh}\frac{L}{R} + \text{arsinh}\frac{R}{L}\right]. \tag{A8}
\end{aligned}$$

We see that $V(0)$ is finite for any $L > 0$, that it diverges as $\log(1/L)$ for $L \to 0$, and that it vanishes for $L \to \infty$. We redefine the potential as

$$\begin{aligned}
\hat{V}(z) &= V(z) - V(0) \\
&= \frac{eQ}{RL}\int_0^R dx\left[\text{arsinh}\left(\frac{L}{\sqrt{x^2 + z^2}}\right) - \text{arsinh}\frac{L}{x}\right].
\end{aligned}$$

Let us consider the asymptotic behaviour of $V(z)$, for $z \to \infty$, for $L$ having any fixed finite value. To this end, we recall that, when $u = L/\sqrt{x^2 + z^2} \to 0$, we can approximate arsinh with its Taylor expansion $\text{arsinh}(u) = u - u^3/6 + O(u^5)$; retaining only the first term, we have

$$V(z) = \frac{eQ}{R}\int_0^{R/z}\frac{du}{\sqrt{1 + u^2}} = \frac{eQ}{R}\,\text{arsinh}\frac{R}{z} \simeq \frac{eQ}{z}.$$

We consider now the limit $L \to \infty$: here, it is evident that $V(0) = 0$. Moreover, starting from Equation (A7) and computing the electric field, we have

$$\begin{aligned}
\mathcal{E}_z &= -\frac{\partial V}{\partial z} = 4\sigma\int_0^R dx\frac{1}{\sqrt{1 + \frac{L^2}{x^2 + z^2}}}\frac{Lz}{(x^2 + z^2)^{3/2}} \\
&= 4\sigma\int_0^R \frac{dx}{z}\frac{1}{1 + \frac{x^2}{z^2}}\frac{1}{\left(1 + \frac{x^2 + z^2}{L^2}\right)^{1/2}}.
\end{aligned}$$

If we take the limit for $L \to \infty$, we recover the following result

$$\mathcal{E}_z = 4\sigma\arctan\frac{R}{z}, \quad \mathcal{E}_z \sim \frac{4\sigma R}{z} \quad \text{for } z \to \infty. \tag{A9}$$

As a consequence, the potential behaves as $V(z) \simeq -4\sigma R \log(R/z)$ for $z \to \infty$. We compute exactly the potential corresponding to Eq. (A9), introducing again the dimensionless variable $\zeta = z/R$

$$V(z) = -4\sigma \int_0^z \arctan\frac{R}{z'} \, dz'$$

$$= 4R\sigma \left( -\zeta \arctan\frac{1}{\zeta} + \log\frac{1}{\sqrt{(1+\zeta^2)}} \right), \quad \text{(A10)}$$

where manifestly $V(0) = 0$.

The potential now diverges for $z \to \infty$, but we still use the energy conservation

$$E + eV = 0, \quad E = -eV = E_\infty s(\zeta),$$

where we put, in analogy with the 3D,

$$E_\infty \equiv m\frac{v_\infty^2}{2} = 4eR\sigma$$

$$s(\zeta) = \zeta \arctan\frac{1}{\zeta} - \log\frac{1}{\sqrt{1+\zeta^2}}$$

and Eq. (A5) holds for the coordinate $\zeta$. As in the 3D case, we introduce the coordinate $X = \sqrt{s}$ and Eq. (A6) holds. In order to simplify the analysis, we replace $s(\zeta)$, defined by Eq. (A8), with $s(\zeta) = \log(1 + \zeta)$ which has the same asymptotic behaviour at $\zeta = 0$ and $\zeta \to \infty$. Finally, we have

$$\frac{dX}{d\tau} = \frac{1}{2}\frac{1}{1+\zeta} = \frac{e^{-s}}{2} = \frac{1}{2}e^{-X^2}.$$

The solution reads

$$\tau = 2\int_0^X e^{u^2} \, du = e^{x^2}\left[\frac{1}{x} + \frac{1}{2x^3} + O\left(\frac{1}{x^5}\right)\right].$$

Retaining only the first term, we invert the equation

$$x^2 = \log\tau + \log x, \quad x^2 = \log\tau + \frac{1}{2}\log\log\tau + \cdots.$$

The results is given by

$$E = E_\infty\left[\log\tau + \frac{1}{2}\log\log\tau\right] \quad \tau = t\frac{v_\infty}{R},$$

and neglecting the loglog term, we get the required result.

[1]A. Sgattoni, P. Londrillo, A. Macchi, and M. Passoni, "Laser ion acceleration using a solid target coupled with a low-density layer," Phys. Rev. E **85**, 036405 (2012).

[2]E. d'Humières, A. Brantov, V. Yu. Bychenkov, and V. T. Tikhonchuk, "Optimization of laser-target interaction for proton acceleration," Phys. Plasmas **20**(2), 023103 (2013).

[3]J. Schreiber, F. Bell, F. Grüner, U. Schramm, M. Geissler, M. Schnürer, S. Ter-Avetisyan, B. M. Hegelich, J. Cobble, E. Brambrink, J. Fuchs, P. Audebert, and D. Habs, "Analytical model for ion acceleration by high-intensity laser pulses," Phys. Rev. Lett. **97**, 045005 (2006).

[4]L. A. Gizzi, C. Altana, F. Brandi, P. Cirrone, G. Cristoforetti, A. Fazzi, P. Ferrara, L. Fulgentini, D. Giove, P. Koester, L. Labate, G. Lanzalone, P. Londrillo, D. Mascali, A. Muoio, D. Palla, F. Schillaci, S. Sinigardi, S. Tudisco, and G. Turchetti, "Role of laser contrast and foil thickness in target normal sheath acceleration," Nucl. Instrum. Methods Phys. Res., Sect. A **829**, 144–148 (2016).

[5]M. Borghesi, J. Fuchs, S. V. Bulanov, A. J. Mackinnon, P. K. Patel, and M. Roth, "Fast ion generation by high-intensity laser irradiation of solid targets and applications," Fusion Sci. Technol. **49**(3), 412–439 (2006); available at http://pure.qub.ac.uk/portal/en/publications/fast-ion-generation-by-highintensity-laser-irradiation-of-solid-targets-and-applications(77a8bf2e-c4a8-4d49-a44a-10bbda2388a7)/export.html.

[6]A. Macchi, M. Borghesi, and M. Passoni, "Ion acceleration by super-intense laser-plasma interaction," Rev. Mod. Phys. **85**, 751–793 (2013).

[7]H. Daido, M. Nishiuchi, and A. S. Pirozhkov, "Review of laser-driven ion sources and their applications," Rep. Prog. Phys. **75**(5), 056401 (2012).

[8]S. Fritzler, V. Malka, G. Grillon, J. P. Rousseau, F. Burgy, E. Lefebvre, E. d'Humiéres, P. McKenna, and K. W. D. Ledingham, "Proton beams generated with high-intensity lasers: Applications to medical isotope production," Appl. Phys. Lett. **83**(15), 3039–3041 (2003).

[9]T. Ceccotti, A. Lévy, H. Popescu, F. Réau, P. D'Oliveira, P. Monot, J. P. Geindre, E. Lefebvre, and Ph. Martin, "Proton acceleration with high-intensity ultrahigh-contrast laser pulses," Phys. Rev. Lett. **99**, 185002 (2007).

[10]K. Zeil, S. D. Kraft, S. Bock, M. Bussmann, T. E. Cowan, T. Kluge, J. Metzkes, T. Richter, R. Sauerbrey, and U. Schramm, "The scaling of proton energies in ultrashort pulse laser plasma acceleration," New J. Phys. **12**(4), 045015 (2010).

[11]I. Spencer, K. W. D. Ledingham, P. McKenna, T. McCanny, R. P. Singhal, P. S. Foster, D. Neely, A. J. Langley, E. J. Divall, C. J. Hooker, R. J. Clarke, P. A. Norreys, E. L. Clark, K. Krushelnick, and J. R. Davies, "Experimental study of proton emission from 60 fs, 200 mJ high-repetition-rate tabletop-laser pulses interacting with solid targets," Phys. Rev. E **67**, 046402 (2003).

[12]D. Neely, P. Foster, A. Robinson, F. Lindau, O. Lundh, A. Persson, C.-G. Wahlström, and P. McKenna, "Enhanced proton beams from ultrathin targets driven by high contrast laser pulses," Appl. Phys. Lett. **89**(2), 021502 (2006).

[13]A. Yogo, H. Daido, S. V. Bulanov, K. Nemoto, Y. Oishi, T. Nayuki, T. Fujii, K. Ogura, S. Orimo, A. Sagisaka, J.-L. Ma, T. Zh. Esirkepov, M. Mori, M. Nishiuchi, A. S. Pirozhkov, S. Nakamura, A. Noda, H. Nagatomo, T. Kimura, and T. Tajima, "Laser ion acceleration via control of the near-critical density target," Phys. Rev. E **77**, 016401 (2008).

[14]A. Flacco, F. Sylla, M. Veltcheva, M. Carrié, R. Nuter, E. Lefebvre, D. Batani, and V. Malka, "Dependence on pulse duration and foil thickness in high-contrast-laser proton acceleration," Phys. Rev. E **81**, 036405 (2010).

[15]P. Londrillo, A. Marocchino, A. Sgattoni, and S. Sinigardi, *ALaDyn* (Zenodo, 2016).

[16]P. Mora, "Plasma expansion into a vacuum," Phys. Rev. Lett. **90**, 185002 (2003).